Intradimer / intermolecular interactions suggest auto-inhibition mechanism in endophilin A1

Zhiming Chen[1], Ken Chang[1], Benjamin R. Capraro[1], Chen Zhu[1], Chih-Jung Hsu[1], Tobias Baumgart[1,*]

[1] Department of Chemistry, University of Pennsylvania, 231 S. 34th St., Philadelphia, PA 19104, USA.

Supplemental material

Materials. 4-(2-hydroxyethyl)-1-piperazineethanesulfonic acid (HEPES) and polyethylene glycol (PEG) were from SIGMA-ALDRICH® (St. Louis, MO); sodium chloride (NaCl) was from Fisher Scientific (Fair Lawn, NJ); tris (2-carboxyethyl) phosphine (TCEP), Coomassie plus (Bradford) protein assay reagent, and bovine serum albumin (BSA) standards were from Pierce/Thermo Fisher Scientific (Rockford, IL); the dyes Pacific Blue™ (PB) C5-maleimide, Alexa Fluor® 488 (AF-488) C5-maleimide, and Texas Red 1,2-Dihexadecanoyl-sn-Glycero-3-Phosphoethanolamine, Triethylammonium Salt (Texas Red DHPE) were from Invitrogen/Life Technologies (Carlsbad, CA); casein was obtained from Fisher Scientific (Rochester, NY); urea was from Fisher BioReagents (Pittsburgh, PA). 1,2-dioleoyl-sn-glycero-3-phosphocholine (DOPC), 1,2-dioleoyl-sn-glycero-3-phospho-L-serine (DOPS), 1,2-dioleoyl-sn-glycero-3-phosphoethanolamine (DOPE) and L-α-phosphatidylinositol-4,5-bisphosphate (PI(4,5)P2) were from Avanti Polar Lipids (Alabaster, AL).

Protein Preparation. A plasmid encoding rat endophilin A1 (obtained from P. De Camilli, Yale) was used to generate endo_N-BAR , endo_dH0 and endo_dSH3 mutants. All of these, including the full length protein, contained a single cysteine introduced at position 241, for details see ref. (*1*). Proteins were purified as described (*1*). Briefly, BAR domains were affinity-purified (via cleavable GST), then subjected to ion exchange and size exclusion chromatography, and stored after flash-freezing. Before measurements, supernatant portions from ultracentrifugation of thawed samples were selected and solution concentrations determined as described (*1*). Note that concentrations considered below refer to endo_N-BAR subunits (i.e. monomers rather than dimers). All proteins were labeled with cysteine-reactive (maleimide-) dyes as described, and unreacted dye was removed by HiTrap Desalting columns (GE) (*1*). Dual-labeled protein was prepared by incubating proteins with a dye mixture (PB/AF488 mole fraction = 0.5). The labeling efficiency for both fluorophores was determined through absorption measurements. AF 488's concentration can be determined from its absorbance peak value since PB's contribution to the AF488 absorbance peak is negligible. PB's concentration could be determined after

subtracting the contribution of AF488 to PB's absorbance peak. Dye concentrations thus determined, together with measured protein concentrations yield the labeling ratios.

Casein Passivation. The loss of protein due to surface adsorption during sample preparation and measurements affects the accuracy of our measurements, particularly at low protein concentrations. Therefore, several methods (including passivation through incubation with casein, BSA, and PEG, respectively) were evaluated for passivation of cuvettes, tips and tubes used in our measurements. From this comparison (data not shown), we found that passivation with casein was the most efficient method of preventing protein loss, to less than 3% in 1.5 hours. Thus, casein passivation was used for all of our measurements as follows. Dried casein was dissolved in buffer solution at 5 mg/ml, and the solution was filtered before use. The casein solution was applied to 1.5 ml tubes, pipette tips, and quartz cuvettes, followed by incubation for 1 hour at room temperature. The casein solution was then removed and the tubes, tips and cuvettes were rinsed two times with buffer solution.

To demonstrate the effectiveness of this passivation procedure, excitation scans of endo_N-BAR _C241-AF-488 (monitoring emission at 519 nm) were acquired as a function of target total subunit concentration without casein passivation (Fig. S1A) and with casein passivation (Fig. S1B). Significant deviation from a linear trend for low concentrations in Fig. S1A indicates protein loss most likely due to surface adsorption during sample preparation and measurements. The comparison to Fig. S1B shows that casein passivation effectively reduces this protein loss.

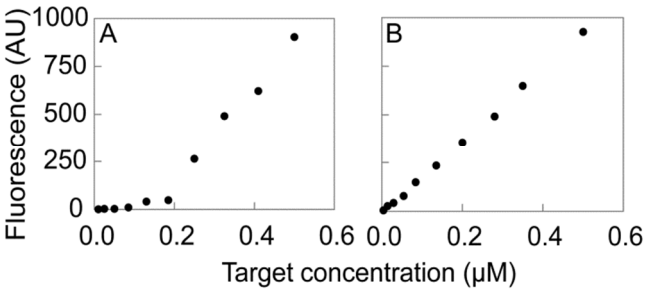

Figure S1. Casein passivation can effectively reduce loss of endo_N-BAR during incubation and measurements. *A*, Fluorescence emission as a function of total subunit concentration obtained without casein passivation. Endo_N-BAR _C241-AF-488 was excited at 495 nm, and emission was measured at 519 nm. *B*, Same conditions as those in (*A*), except for casein passivation being applied.

Fluorimetry Measurements. Both kinetic and equilibrium fluorimetry measurements were performed with a Cary Eclipse Fluorescence Spectrophotometer with a Peltier-controlled temperature block. In the *Förster resonance energy transfer* (*FRET*) measurements, Endo_N-BAR _C241-PB served as donor and Endo_N-BAR _C241-AF-488 as acceptor. The ratio of donor/acceptor was chosen as 0.5 to promote FRET (*1*). The peak values of the emission spectra (455 nm for PB and 519 nm for AF-488) and the peak value of the excitation spectrum of AF-488 (495 nm) were chosen for analysis. Proteins were incubated in 150 mM NaCl, 20 mM HEPES, 1 mM TCEP, pH 7.4 buffer solution.

Kinetic Measurements. Kinetic measurements determined the dissociation rate constant, k_{off}, for endo_N-BAR dimerization. Both donor and acceptor samples were diluted separately with buffer such that the final total subunit concentration was 2 μM in each. Then two samples were pre-incubated at the temperature of interest until they had fully reached monomer/dimer equilibrium, as determined by FRET studies. The following incubation times and incubation temperatures were chosen: 40 hours for 22 ºC, 9 hours at 27 ºC, 3 hours at 30 ºC, 1 hour at 32 ºC, 18 minutes at 35 ºC, and 10 minutes at 37 ºC. The equilibrated endo_N-BAR samples were combined (total endo_N-BAR subunit concentration remained 2 μM after combination, donor to acceptor ratio was adjusted to 0.5), and mixed by pipetting up and down. An excitation scan was taken immediately after mixing, followed by sequential emission scans to monitor FRET. The duration of the time series was the same as the pre-incubation period. Afterwards, a second excitation scan was taken to ensure that the endo_N-BAR concentration remained constant throughout the experiment. As detailed below, at higher temperatures, the kinetics of subunit exchange is much faster than at lower temperature points. Thus, at high temperatures significant monomer exchange might occur already during the first excitation scan. To avoid this problem for the highest temperatures considered, the

sequential emission scans were taken immediately after mixing the two differently labeled protein samples at 35 ºC and 37 ºC. Via excitation scans using a second sample in a separate cuvette, we ensured absence of significant protein loss during measurements at 35 ºC and 37 ºC. From the comparison of the peak of the excitation spectrum at 495 nm preceding and following the time series (a representative example is shown in Fig. S2A), we ensured that protein concentration change was <5% for all temperature trials.

We choose measurements at the temperature of 37 ºC to demonstrate the protocol for data analysis. In the analysis, the average fluorescence intensity over a wavelength range of 8 nm in the neighborhood of the peak wavelength was used.

The time dependence of donor quenching at 455 nm (see arrow in Fig. S2B) is plotted in Fig. S2C. FRET efficiency was calculated according to,

$$E = 1 - \frac{F_{DA}}{F_D} \ , \qquad \text{(S1)}$$

where F_D is the peak initial donor fluorescence and F_{DA} is the donor fluorescence (in the presence of the acceptor) at the time point of interest. The calculated FRET efficiency is graphed in Fig. S2D. Assuming a two-step process for endo_N-BAR association/dissociation, it can be shown that monomer exchange kinetics (and thus the time dependence of the FRET signal) depend only on k_{off} (*1-3*), according to:

$$E = E_{inf}\,(1 - e^{-t*k_{off}}), \qquad \text{(S2)}$$

where E_{inf} is the FRET efficiency limit (FRET efficiency at $t = \infty$). Fitting Eq. S2 to the FRET efficiency values (Fig. S2D) yields k_{off} = 7.63×10^{-3} s^{-1} and E_{inf} = 41.6% for this measurement at 37ºC.

For the measurements just described, endo_N-BAR domains were labeled with two fluorophores (PB and AF-488). It is important to evaluate the potential influence of the fluorescent labels on the kinetics of endo_N-BAR dimerization/dissociation. We therefore asked the question if the presence of labels on

endo_N-BAR alter the kinetics of protein dimerization/dissociation. In the absence of such an effect, the overall equilibrium between dimers and monomers will not be perturbed through labeling (*3*). To answer this question, a kinetic measurement at 37 ºC was carried out to monitor the monomer exchange kinetics of unlabeled and labeled endo_N-BAR.

For this purpose, the following solutions were separately equilibrated at 37 ºC: a 2 μM solution of dual-labeled endo_N-BAR (labeled both with PB and AF488 at a measured ratio of D/A = 0.44) and a second solution of unlabeled endo_N-BAR (2 μM). After monomer/dimer equilibrium was established at this temperature, the two solutions were quickly combined and sequential emission scans were obtained. The initial scan showed maximal FRET. With increasing time, the FRET efficiency decreased, showing an increase in the donor emission at the emission maximum of the donor (λ_{em}^{D} = 455 nm) (Fig. S2E), which was termed *donor dequenching* here. The extent of *donor dequenching*, E', shown in Fig. S2F, was fitted with Eq. S2 (with E exchanged by E'), yielding k_{off} = 6.15×10^{-3} s^{-1} (i.e. comparable to the value found for the donor quenching experiment), and E'_{inf}= 17.9% (i.e. close to half of E_{inf} 41.6% determined in the donor quenching experiments, as expected).

Kinetic measurements of endo_N-BAR dissociation in urea solution were carried out at 27 ºC. endo_N-BAR _C241-PB and endo_N-BAR _C241-AF-488 were equilibrated separately in 0 M, 0.25 M, 0.5 M, 0.75 M, and 1 M urea buffer solution, respectively, and then mixed. A sequential emission scan (as shown in materials and methods, kinetic measurements) was taken immediately after mixing, to assess the FRET signal. The resulting trends of FRET efficiency with respect to time was fit with a two parameter model to obtain k_{off}.

Kinetic measurements of endo_FL dissociation in urea solution were carried out at 37 ºC. Endo_FL _C241-PB and endo_FL _C241-AF-488 were equilibrated separately in 0.75 M, 1 M, 1.25M urea buffer solution, respectively, and then mixed. A sequential emission scan was taken immediately after mixing, to

assess the FRET signal. The resulting trends of FRET efficiency with respect to time was fit with a two parameter model to obtain k_{off}.

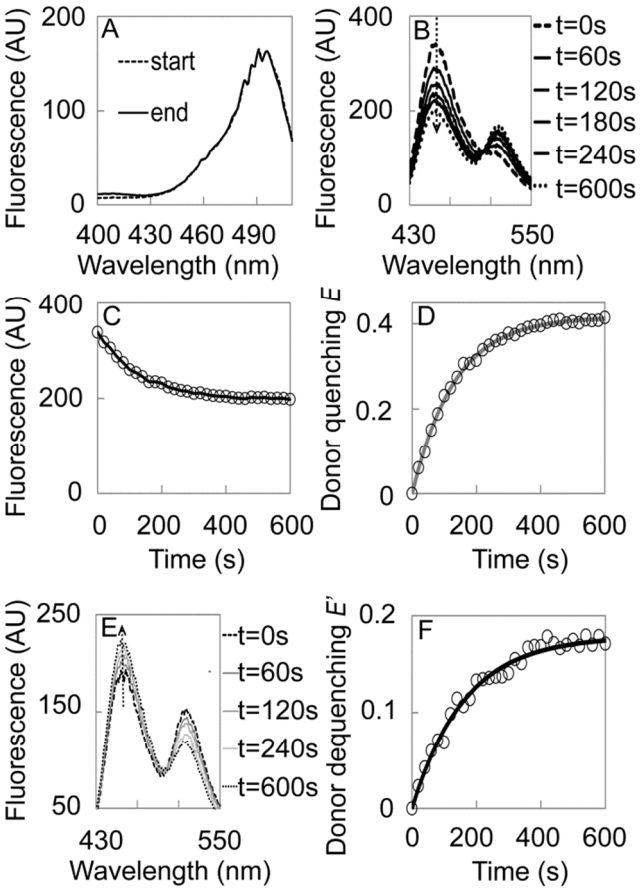

Figure S2. FRET kinetic experiment protocol for endo_N-BAR monomer exchange. *A*, Excitation scans of mixed endo_N-BAR _C241-PB and endo_N-BAR _C241-AF-488 collected before and after a series of emission scans as described in the main text, D/A = 0.5 and 2 μM total protein, at 37ºC. *B*, Sequential emission scans (every 20 seconds) of same sample as (*A*) at 37ºC. *C*, Fluorescence intensity from (*B*) at the wavelength indicated by the dashed arrow records the donor quenching signal. *D*, FRET efficiency calculated from donor quenching, fluorescence relative to the initial value in (*C*), with single-exponential fit (line) yielding k_{off} = 7.63×10^{-3} s^{-1}, E_{inf} = 41.6% (using Eq. 3). *E*, Sequential emission scans (every

20 seconds) of a mixed sample with dual-labeled endo_N-BAR (C241-PB and C241-AF-488, D/A = 0.44 sample and unlabeled endo_N-BAR, dual-labeled/unlabeled = 1:1 and 2 μM total protein, at 37 ºC. *F*, Fluorescence intensity from (*E*) at the wavelength indicated by the dashed arrow allows calculation of the dequenching extent, E' relative to the initial intensity. A single-exponential fit (line) yielded k_{off} = $6.15\times10^{-3}\,s^{-1}$, E'_{inf}= 17.9%.

Equilibrium Measurements. The goal of equilibrium FRET measurements was to determine the dissociation constant, K_D, of ENBAR. As for kinetic measurements, casein passivation was used. In order to further reduce experimental errors resulting from pipetting and adsorption, we determined donor and acceptor content of mixed samples from fluorescence measurements. The procedure to quantify sensitized emission in the mixed sample and to relate it to endo_N-BAR dimerization affinity is related to the procedure described in Refs (*4, 5*).

Fig. S3A and S3B shows the emission and excitation scans, respectively, of a mixed sample FRET pair, a donor-only sample and an acceptor-only sample (*5*). The concentrations of the donor and acceptor in the respective standard solutions were identical to the values in the mixed sample. Fig. S3A indicates that donor-only emission (blue line) is maximal at λ^D_{em}, while the acceptor-only emission (red line) at λ^D_{em} is negligible. The emission at λ^D_{em}, therefore, arises entirely from the donor. Excitation scans (Fig. S3B) reveal that the excitation of the acceptor-only sample (green line) is maximal at λ^A_{ex}, which is an excitation wavelength leading to negligible donor excitation (Fig. S3B, blue line). This means that measured emission at λ^A_{ex}, upon direct excitation of the acceptor, is due to the acceptor only. Additionally, note that the emission spectrum of the mixed sample (Fig. S3A, green line) has two peaks.

As shown above, the fluorescence at λ^D_{em} of a donor / acceptor mixture arises from donor fluorescence only. However, the fluorescence intensity $F_{em}(\lambda^A_{em})$ of a mixed sample has three sources: a direct donor contribution, $F_{DA}(\lambda^A_{em})$; a direct acceptor contribution, $F_A(\lambda^A_{em})$; and the sensitized emission of the acceptor, $F_{sen}(\lambda^A_{em})$. These relationships are shown below:

$$F_{em}(\lambda_{em}^{A}) = F_{AD}(\lambda_{em}^{A}) + F_{DA}(\lambda_{em}^{A}) , \quad \text{(S3)}$$

$$F_{AD}(\lambda_{em}^{A}) = F_{A}(\lambda_{em}^{A}) + F_{sen}(\lambda_{em}^{A}) . \quad \text{(S4)}$$

Here, $F_{AD}(\lambda_{em}^{A})$ is the total acceptor emission at λ_{em}^{A} (in the presence of the donor).

The observations above indicate that emission scans of the donor-only sample and excitation scans of the acceptor-only sample can be used to calculate the direct contribution of donor and acceptor in emission spectra of mixed samples, and, further, to obtain the amount of FRET for each sample (*5*). To perform equilibrium measurements, a donor-only standard and an acceptor-only standard were prepared as well as ten mixed samples with varying concentrations (*4*). To keep the acceptor fraction constant across individual concentration points, the most concentrated sample of the series with mixed donor and acceptor was prepared and then diluted to the additional nine desired concentrations. To establish monomer-dimer equilibrium, the samples were incubated at specific temperatures for equilibration times indicated by kinetic measurements. For each sample, two scans were obtained: an excitation scan from 450 nm to 508 nm with an emission wavelength at 519 nm, and an emission scan from 420 nm to 580 nm with an excitation wavelength 400 nm. For all excitation and emission spectra, any buffer contribution was subtracted from all sample spectra.

Fig. S3C-F shows the data processing protocol for equilibrium measurements in detail (*5*). Firstly, as shown in Fig. S3C, the comparison of the acceptor standard excitation spectrum, $F_{A,\,ex}^{S}$, and the mixed sample excitation spectrum, F_{ex}, (both at the wavelength λ_{ex}^{A} of maximal acceptor excitation) yields the ratio,

$$\frac{F_{ex}(\lambda_{ex}^{A})}{F_{A,\,ex}^{S}(\lambda_{ex}^{A})} = R_A . \quad \text{(S5)}$$

From this ratio, the direct acceptor contribution to the emission spectrum of a mixed sample can be calculated as follows (Fig. S3D):

$$F^{S}_{A,\,em} * R_A = F_A. \quad \text{(S6)}$$

Here, $F^{S}_{A,\,em}$ and F_A are emission spectra of the acceptor standard, and the calculated emission due to direct excitation of acceptor in the mixed sample, respectively. As a result, the emission spectrum, F_A, from direct acceptor excitation at λ^A_{em}, can be subtracted from the emission spectrum of the mixed sample.

Secondly, to subtract the donor emission from the spectrum of the mixed sample, a comparison of donor standard emission spectrum, $F^{S}_{D,\,em}$, and mixed sample emission spectrum, F_{em}, yields the ratio (Fig. S3E),

$$\frac{F_{em}(\lambda^D_{em})}{F^{S}_{D,\,em}(\lambda^D_{em})} = R_D. \quad \text{(S7)}$$

As a result, the contribution of donor emission in the spectrum of the mixed sample can be calculated (Fig. S3F):

$$F^{S}_{D,\,em} * R_D = F_{DA}. \quad \text{(S8)}$$

Accordingly, both the contributions from acceptor emission through direct excitation, F_A, and donor emission, F_{DA}, can be accounted for. According to Eqs. (S3-4), $F_{sen}(\lambda^A_{em})$ (Fig. S3F) can be calculated by subtraction of $F_A(\lambda^A_{em})$ and $F_{DA}(\lambda^A_{em})$ from $F_{em}(\lambda^A_{em})$, to allow calculation of $\frac{F_{sen}(\lambda^A_{em})}{F_A(\lambda^A_{em})}$ for each sample.

We note that under conditions where the acceptor fraction (ratio of acceptor-labeled proteins relative to total protein concentration) is constant, this ratio is directly proportional to the FRET efficiency. We monitor $\frac{F_{sen}(\lambda^A_{em})}{F_A(\lambda^A_{em})}$ with respect to varied total protein concentrations C_T and fit the results with the following equation (*4*),

$$\frac{F_{sen}(\lambda^A_{em})}{F_A(\lambda^A_{em})} = A\frac{4C_T + K_D - \sqrt{K_D^2 + 8C_T K_D}}{4C_T}, \quad \text{(S9)}$$

which yields the dissociation constant, K_D, and the value of A (which is the $\frac{F_{sen}(\lambda_{em}^A)}{F_A(\lambda_{em}^A)}$ value for an infinitely large C_T).

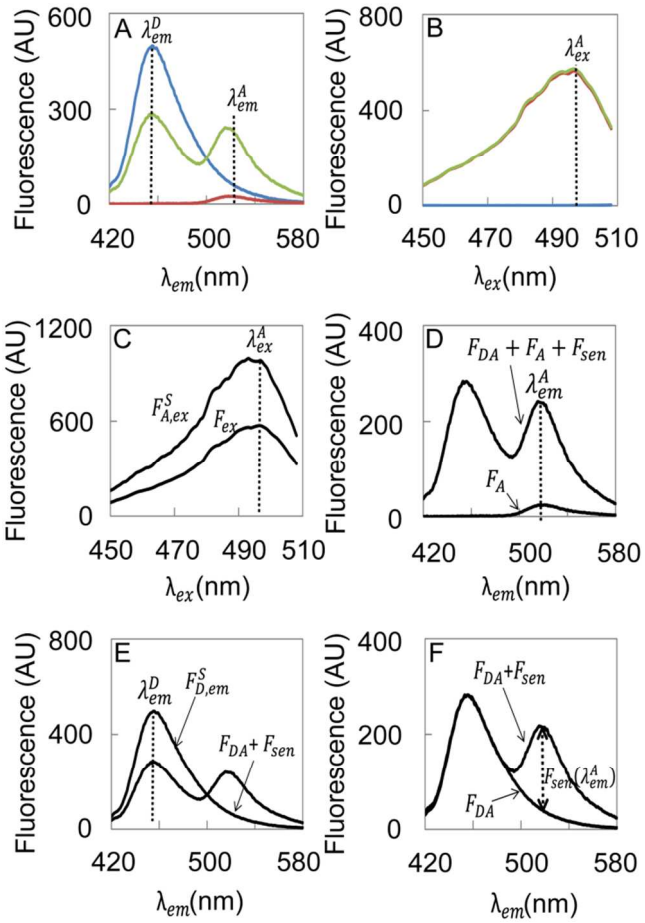

Figure S3. Emission and excitation scans of two standards and a mixed sample. Green: Mixed sample (donor/acceptor = 0.5), total protein concentration 0.3μM; blue: donor only standard; red: acceptor only standard. Concentration of the donor and acceptor in the respective standard solutions were the same as in the mixed sample. Buffer: 20mM HEPES, 150mM NaCl, 1mM TCEP, pH = 7.4. *A*, Emission scans (excitation at 400 nm) reveal that acceptor emission at λ_{em}^D is negligible. *B*, Excitation scans (emission collected at 519 nm) reveal that donor excitation at λ_{ex}^A is negligible. All spectra in both (*A*) and (*B*) are averaged from 10 scans (after blank subtraction). *C*, Comparison of the excitation spectra of sample, F_{ex},

and acceptor standard $F^{S}_{A,\,ex}$, yields a ratio, R_A, by equation (S5). *D*, Calculation of the direct acceptor contribution, F_A, via equation (S6). *E*, Comparison of the emission spectrum of each sample and donor standard yields another ratio,R_D, according to equation (S7). *E*, Calculation of the direct donor contribution, F_{DA}, via equation (S8) determines the sensitized emission, $F_{sen}(\lambda^{A}_{em})$.

Association Rate Constant of endo_N-BAR

The monomer association rate constant of Endo_N-BAR is calculated from the ratio of dissociation rate constant, k_{off}, and dissociation constant, K_D.

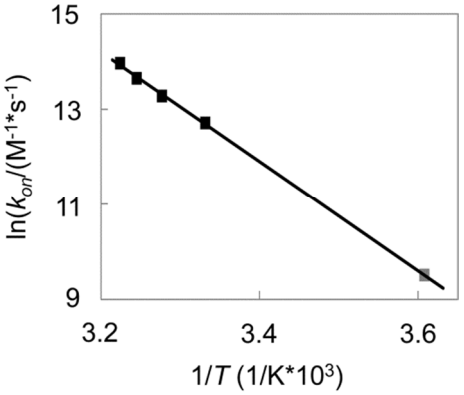

Figure S4. The natural logarithm of the association rate constant depends linearly on the reciprocal temperature.

Comparison of binding capacity of endophilin constructs

To compare the membrane binding capacity among endophilin constructs, we have measured the membrane binding fluorescence intensity of different endophilin truncation constructs by adding the same concentration of endo_FL, endo_N-BAR, endo_dSH3 and endo_dH0 into GUV dispersions with identical lipid concentrations (composition 24.5% DOPC + 35% DOPS + 30% DOPE + 10% PI(4,5)P2, +0.5% TexasRed-DHPE). Figure S5, shows that no significant difference in membrane binding capacity was observed for endo_N-BAR and endo_dSH3. However, endo_FL showed significantly lower membrane

binding capacity compared endo_N-BAR (the fluorescence intensity of endo_FL is ~ 35% of that of endo_N-BAR). This observation is consistent with a hypothesized auto-inhibition for full-length endophilin. Figure S5 also shows that the membrane binding capacity of endo_dH0 is substantially smaller than that of endo_FL. The significantly weaker binding capacity in the absence of the H0 helix is consistent with literature findings since the H0 helix is known to insert into the membrane during membrane association and to significantly contribute to the membrane binding capacity of endophilin by mediating its oligomerization on the membrane (*6, 7*).

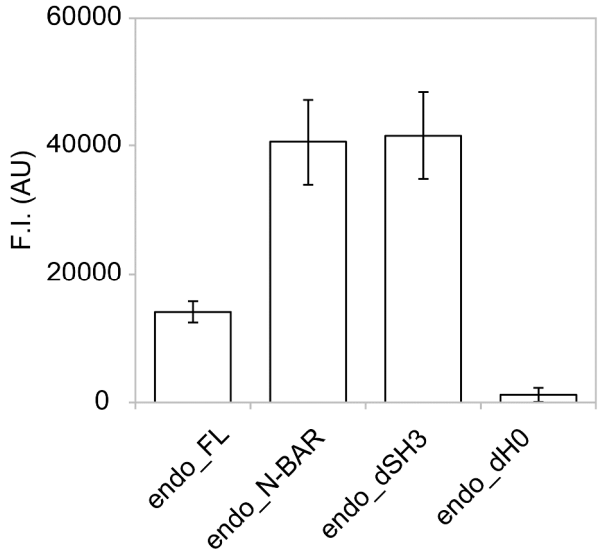

Figure S5. The protein fluorescence intensity of endo_FL, endo_N-BAR, endo_dSH3, and endo_dH0, bound to GUV membranes. All endophilin constructs were labeled with Alexa fluor 488. GUVs were prepared with the composition of 24.5% DOPC, 35% DOPS, 30% DOPE, 10% DOPS and 0.5% Texas Red-DHPE. The protein concentrations for different constructs were kept to be identical at 100 nM, and the lipid concentration was kept at 18.5 μM for all trials. The numbers of GUVs used to obtain these results was 26, 22, 18 and 17, respectively.

Reference

1. Capraro, B. R., Shi, Z., Wu, T. T., Chen, Z. M., Dunn, J. M., Rhoades, E., and Baumgart, T. (2013) Kinetics of Endophilin N-BAR Domain Dimerization and Membrane Interactions, *Journal of Biological Chemistry 288*, 12533-12543.

2. Wendt, H., Berger, C., Baici, A., Thomas, R. M., and Bosshard, H. R. (1995) Kinetics of Folding of Leucine-Zipper Domains, *Biochemistry-Us 34*, 4097-4107.
3. Jonsson, T., Waldburger, C. D., and Sauer, R. T. (1996) Nonlinear free energy relationships in arc repressor unfolding imply the existence of unstable, native-like folding intermediates, *Biochemistry-Us 35*, 4795-4802.
4. Jia, H. F., Satumba, W. J., Bidwell, G. L., and Mossing, M. C. (2005) Slow assembly and disassembly of lambda Cro repressor dimers, *J. Mol. Biol. 350*, 919-929.
5. Merzlyakov, M., Chen, L., and Hristova, K. (2007) Studies of receptor tyrosine kinase transmembrane domain interactions: The EmEx-FRET method, *J Membrane Biol 215*, 93-103.
6. Capraro, B. R., Shi, Z., Wu, T., Chen, Z., Dunn, J. M., Rhoades, E., and Baumgart, T. (2013) Kinetics of Endophilin N-BAR Domain Dimerization and Membrane Interactions, *J Biol Chem 288*, 12533-12543.
7. Mim, C., Cui, H. S., Gawronski-Salerno, J. A., Frost, A., Lyman, E., Voth, G. A., and Unger, V. M. (2012) Structural Basis of Membrane Bending by the N-BAR Protein Endophilin, *Cell 149*, 137-145.